Experimental observation and analysis of all-fiber plasmonic double Airy beams

Chunying Guan,[1,2,*] Ming Ding,[2] Jinhui Shi,[1] Ping Hua,[2] Pengfei Wang,[2,3] Libo Yuan,[1] and Gilberto Brambilla[2]

[1]*Key laboratory of In-fiber Integrated Optics of Ministry of Education, College of Science, Harbin Engineering University, Harbin 150001, China*

[2]*Optoelectronics Research Centre, University of Southampton, Southampton SO17 1BJ, UK*

[3]*Photonics Research Centre, Dublin Institute of Technology, Kevin Street, Dublin 8, Ireland*

[*]*cyguan@163.com*

Abstract: The propagation dynamics of all-fiber plasmonic double parallel and orthogonal Airy beams are experimentally demonstrated. Two slits and groove arrays were fabricated by focused ion beam (FIB) milling on the gold coated end facet of an optical fiber to generate two Airy beams simultaneously. Sub-wavelength self-focusing of double parallel Airy beams in free space is experimentally verified. Effects of geometrical parameters on the intensity profiles of the focal spot are analyzed in detail. The characteristics at the junction of the two main lobes can be adjusted by controlling the initial phase difference of the two Airy beams. The propagation of two orthogonal Airy beams is also experimentally investigated. Multi-Airy beams are of importance to realize all-fiber optical trapping, fiber integrated devices, and laser shaping.

OCIS codes: (060.2340) Fiber optics components; (240.6680) Surface plasmons; (050.6624) Subwavelength structures; (230.3120) Integrated optics devices; (140.3300) Laser beam shaping.

References and links

1. K. Dholakia and T. Čižmár, "Shaping the future of manipulation," Nat. Photonics **5**(6), 335–342 (2011).
2. W. M. Lee, X.-C. Yuan, and W. C. Cheong, "Optical vortex beam shaping by use of highly efficient irregular spiral phase plates for optical micromanipulation," Opt. Lett. **29**(15), 1796–1798 (2004).
3. D. G. Grier, "A revolution in optical manipulation," Nature **424**(6950), 810–816 (2003).
4. A. Mathis, F. Courvoisier, L. Froehly, L. Furfaro, M. Jacquot, P. A. Lacourt, and J. M. Dudley, "Micromachining along a curve: Femtosecond laser micromachining of curved profiles in diamond and silicon using accelerating beams," Appl. Phys. Lett. **101**(7), 071110 (2012).
5. I. Epstein and A. Arie, "Arbitrary Bending plasmonic light waves," Phys. Rev. Lett. **112**(2), 023903 (2014).
6. J. Baumgartl, M. Mazilu, and K. Dholakia, "Optically mediated particle clearing using Airy wavepackets," Nat. Photonics **2**(11), 675–678 (2008).
7. I. M. Besieris and A. M. Shaarawi, "A note on an accelerating finite energy Airy beam," Opt. Lett. **32**(16), 2447–2449 (2007).
8. G. A. Siviloglou, J. Broky, A. Dogariu, and D. N. Christodoulides, "Observation of accelerating Airy beams," Phys. Rev. Lett. **99**(21), 213901 (2007).
9. P. Zhang, J. Prakash, Z. Zhang, M. S. Mills, N. K. Efremidis, D. N. Christodoulides, and Z. Chen, "Trapping and guiding microparticles with morphing autofocusing Airy beams," Opt. Lett. **36**(15), 2883–2885 (2011).
10. D. G. Papazoglou, N. K. Efremidis, D. N. Christodoulides, and S. Tzortzakis, "Observation of abruptly autofocusing waves," Opt. Lett. **36**(10), 1842–1844 (2011).
11. P. Polynkin, M. Kolesik, J. V. Moloney, G. A. Siviloglou, and D. N. Christodoulides, "Curved plasma channel generation using ultraintense airy beams," Science **324**(5924), 229–232 (2009).
12. G. A. Siviloglou, J. Broky, A. Dogariu, and D. N. Christodoulides, "Ballistic dynamics of Airy beams," Opt. Lett. **33**(3), 207–209 (2008).
13. Y. Fan, J. Wei, J. Ma, Y. Wang, and Y. Wu, "Tunable twin Airy beams induced by binary phase patterns," Opt. Lett. **38**(8), 1286–1288 (2013).
14. A. P. Hibbins, B. R. Evans, and J. R. Sambles, "Experimental verification of designer surface plasmons," Science **308**(5722), 670–672 (2005).
15. A. Minovich, A. E. Klein, N. Janunts, T. Pertsch, D. N. Neshev, and Y. S. Kivshar, "Generation and near-field imaging of Airy surface plasmons," Phys. Rev. Lett. **107**(11), 116802 (2011).

#213846 - $15.00 USD Received 11 Jun 2014; revised 9 Jul 2014; accepted 10 Jul 2014; published 22 Jul 2014

16. L. Li, T. Li, S. M. Wang, C. Zhang, and S. N. Zhu, "Plasmonic Airy Beam generated by in-plane diffraction," Phys. Rev. Lett. **107**(12), 126804 (2011).
17. I. Dolev, I. Epstein, and A. Arie, "Surface-plasmon holographic beam shaping," Phys. Rev. Lett. **109**(20), 203903 (2012).
18. C. Y. Guan, M. Ding, J. H. Shi, P. F. Wang, P. Hua, L. B. Yuan, and G. Brambilla, "Compact all-fiber plasmonic Airy-like beam generator," Opt. Lett. **39**(5), 1113–1116 (2014).
19. H. F. Schouten, N. Kuzmin, G. Dubois, T. D. Visser, G. Gbur, P. F. A. Alkemade, H. Blok, G. W. Hooft, D. Lenstra, and E. R. Eliel, "Plasmon-assisted two-slit transmission: Young's experiment revisited," Phys. Rev. Lett. **94**(5), 053901 (2005).

1. Introduction

Beam shaping techniques provide unique light patterns that play a major role in the field of particle micromanipulation, optical trapping and laser micromachining [1–4]. The generation of self-accelerating light beams along arbitrary caustic curvature has been demonstrated [5]. Airy beams have attracted great attention because of their unusual properties such as non-diffracting, self-accelerating and self-healing [6, 7]. The first accelerating Airy beam was observed in 2007 [8]. Such beams can persist over very long lengths, allowing the extended guiding of objects using the scattering force. Research efforts on Airy beams have expended from fundamental aspects to demonstrations of possible applications. Single [8], circular [9, 10], and 2-D Airy beams [11] have been demonstrated experimentally. While mathematically the Airy beams have infinite energy, in practice only truncated Airy beams of finite energy exist. In most experiments, Airy beams were mainly induced by continuous cubic phase patterns generated using a phase-type spatial light modulator (SLM) [8, 9, 12]. However, the SLM has disadvantages, such as large size, low resolution, and low laser damage threshold [13]. Surface plasmon polaritons (SPPs) offer valuable platforms for many applications due to their relatively long propagation distance and strong confinement to the surface [14]. Plasmonic Airy beam generators have been demonstrated experimentally in planar dimensions, such as a metal film surface with a nanoarray [15, 16]. In these systems, experimental set-ups require extremely precise alignment in free space. Dolev et al have shown that free space Airy beams can be formed by employing computer generated hologram (CGH) of SPPs [17]. Nevertheless, this technique needs a 2f system to optically perform a Fourier transform of the diffracted light. On the contrary, all-fiber Airy beam generators are highly integrated, simple and flexible devices. In our previous work, all-fiber single Airy-like beams have been demonstrated numerically and experimentally, and the non-spreading and self-bending properties have been observed [18].

In this paper, two single Airy beams are simultaneously generated in a parallel or an orthogonal arrangement on the end facet of an optical fiber. The propagation properties of all-fiber multiple plasmonic Airy beams are experimentally and numerically investigated in detail. Sub-wavelength self-focusing of double parallel Airy beams in free space can be obtained. The characteristics at the junction of the two main lobes can be adjusted by controlling the initial phase difference of the two Airy beams.

2. Double parallel Airy beams

2.1 Symmetrical double Airy beams

Figures 1(a)-1(c) show the scanning electron microscope (SEM) images of a fiber-based double parallel Airy beams generator. On the cleaved end of a single mode fiber (SMF) at 980nm (Thorlabs, SM980-5.8-125), a gold film with 200nm thickness was thermally deposited, over which two identical air slits and two 1D graded gratings arrays composed of 35 grooves were engraved by focused ion beam (FIB) (Helios 600, FEI Inc.). The schematic diagram of this sample is shown in Fig. 1(d). Here, h_0 is the thickness of the gold film. Two slits are arranged symmetrically in the fiber core area. The distance d between the two slits is 2.89μm. SPPs are excited in the two air slits, propagate along the metal surface and are decoupled into free space by the graded metal grating arrays [17]. Meanwhile, the surface plasmon polaritons along the

#213846 - $15.00 USD Received 11 Jun 2014; revised 9 Jul 2014; accepted 10 Jul 2014; published 22 Jul 2014

interface between the fiber core and gold film that are excited at one of the slits propagate towards the other slit (dashed arrow in Fig. 1(d)) and forms plasmon-assisted two-slit interference. By optimizing the spatial location and geometric parameters of the grooves, the phase and the amplitude of the decoupling field can well match with that of the Airy beam. The recouping waves of the −1 order diffraction with slightly different diffractive angles superpose in free space and form the desired Airy beam. The details of the optimized method have been described in [18]. The acceleration parameter x_0 of the Airy beam is set as 1.0μm. In the experiment, the slits and grooves widths (w_0 and w) are around 130nm and 260nm, respectively, while their length along the gold surface is ~6μm. The grooves inner surface is not perfectly smooth due to the exposure dose of the ion beams not being perfectly uniform. The depth h of grooves is estimated to be about 60-80nm. The local lattice constant Λ_n of the graded grooves on each side is shown in the inset of Fig. 1(b).

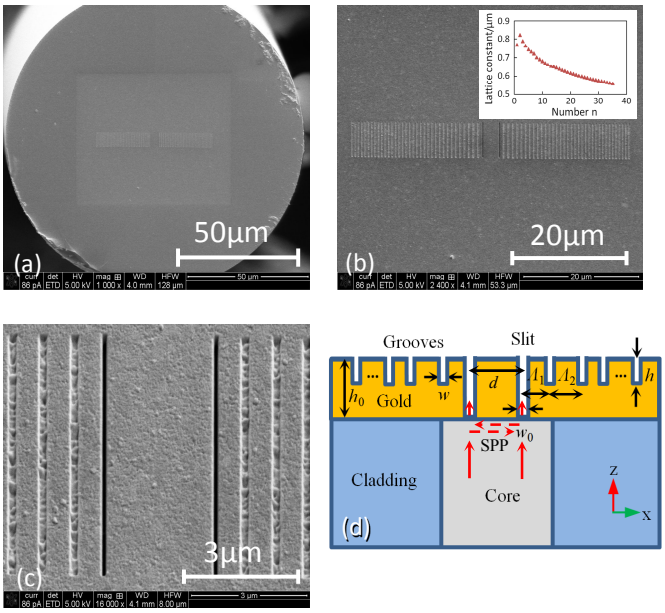

Fig. 1. (a) - (c) SEM images of the nanostructured gold coated optical fiber facet with double parallel slits (d = 2.89 μm) and graded grooves arrays. The inset of Fig. 1(b) is the optimized local lattice constant of the graded grooves. (d) Schematic illustration of the proposed device.

In the test, a 980nm CW laser diode was employed as the incident light source. A fiber polarization rotator was used to control the light polarization state and achieve a polarization perpendicular to the grating lines. Transmitted light was then collected by a microscope objective (100 ×) and the field image was taken by a camera (MicronViewer 7290A) with pixel spacing of 18μm. The cross sections of the captured beam images in the free space at different propagation distances along the z-axis are presented in Fig. 2(a) and the field maps are summarized in Fig. 2(b). Three side lobes of each Airy beam can be clearly observed at z = 1μm. Two symmetrical Airy beams in the free space are transversely accelerated along the opposite directions (+ x and -x), and then interfere and focus at about z = 20μm on the axis of symmetry (x = 0). Furthermore, the double-slit plasmonic interference [19] also contributes to the interference field, which can also be seen in the beam cross section at z = 5μm, where it is not a pure Airy beam. A deformation of the main lobe of Airy beam can be observed, together some discontinuous dark fringes.

A finite-energy Airy beam solution can be written as [6]:

#213846 - $15.00 USD Received 11 Jun 2014; revised 9 Jul 2014; accepted 10 Jul 2014; published 22 Jul 2014

$$E(s,\xi) = \mathrm{Ai}[s-(\xi/2)^2 + ia\xi]\exp[a^3/3 + as - (a\xi^2/2)]\exp[-i(\xi^3/12) + i(a^2\xi/2) + i(s\xi/2)] \quad (1)$$

where $s = x/x_0$, $\xi = z/(kx_0^2)$, a is the exponential truncation factor. A density plot $|E(x, z)|^2$ of two symmetrical Airy beams (x_0 = 1.0μm and a = 0.001) with the separated distance d = 2.9 μm is shown in Fig. 2(c). Two pure Airy beams focus at 20.5μm and then interfere after the focal point. The full-width-at-half-maximum (FWHM) of the focal point is 0.86μm. The phases of two Airy beams at x = 0 are equal, so the junction of the main lobes of two beams is always a bright spot.

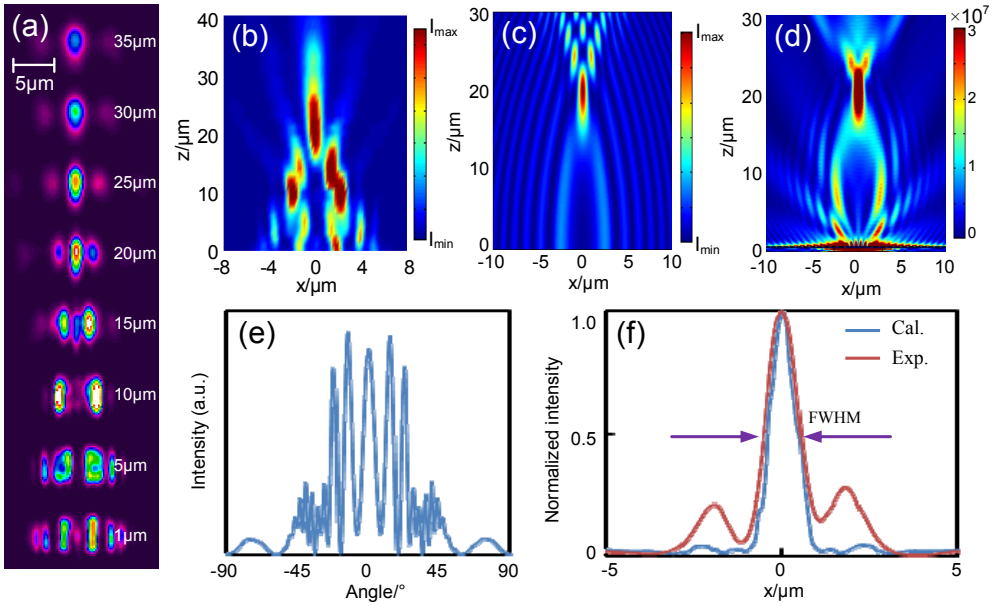

Fig. 2. (a) Cross sections of the beam at different propagation distances for d = 2.89μm. (b) Measured interference field maps in the free space. (c) Calculated interference field maps of two Airy beam by using analytic formula. (d) Calculated interference field maps for the proposed structure by using FEM. (e) Calculated far-field along the x-axis. (f) Intensity profiles of the focal spot.

The numerical calculation for the proposed double plasmonic Airy beams was performed using 2D FEM (COMSOL 3.5a). In the simulations, the numerical aperture (NA) of the fiber is 0.14 and the core diameter is 5.2μm. The cladding is fused silica and its refractive index was calculated by using the Sellmeier equation. TM polarized fundamental mode (i.e. with the electric filed perpendicular to the long axis of the slit) was launched from the lower input port using boundary mode analysis. The intensity distribution of the electric field (d = 2.9μm , h = 75nm) is depicted in Fig. 2(d), showing good agreement between the numerical simulation and measured field maps. The calculated far-field along the x-axis is shown in Fig. 2(e). The far-field intensity is very weak, attributed to the propagation characteristics of finite-energy single Airy beam, which only propagates over a finite distance. Five distinct interference fringes occur between the far-field divergence angles of –25° and 25°. The central fringe is bright, caused by the interference of the two Airy beams after the focal point, which can be seen at z>25μm in Fig. 2(d). The longitudinal position of the focal point is a little longer than that of the experiment due to the limitations associated to measurement precision. The normalized intensity profiles of the focal spot, both experimental and calculated, are shown in Fig. 2(f) and agree well with each other. The experimental and theoretical FWHMs of the focal point are 1.08μm and 0.85μm along the x direction, respectively, which are comparable with the wavelength of the incident light, and less than the calculated FWHM (1.65μm) of the main

#213846 - $15.00 USD Received 11 Jun 2014; revised 9 Jul 2014; accepted 10 Jul 2014; published 22 Jul 2014

lobe. ~7% of the input power can be theoretically achieved around the bright spot. In the experiment the focal spot of the interfering Airy beams is slightly wider than in the simulations. This is attributed to the unwanted scattering, which slightly alters the desired amplitude distribution. As we know, if x_0 takes a smaller value, the main lobe of the Airy beam will become narrower, and then the FWHM of the focal spot will be further reduced. For example, for x_0 = 0.6μm FWHM = 0.46μm.

One also found that the measured intensity profile has two larger side lobes due to the imperfection in the fabrication process. In particular, the non-uniform depth of the grooves greatly affects the amplitude distribution of SPP waves. The effect of the depth of the grooves on the intensity profile of the focal spot is depicted in Fig. 3(a). The results show that the shallow grooves reduce the decay rate of SPPs along the interface and introduce two side lobes with large amplitudes, while the deep grooves widens the focal spot FWHM and enhances the background field. However, the width of the grooves is relatively uniform due to small aspect ratio (75nm/260nm = 0.29) and has a negligible effect on the beam propagation. The field map for the case with h = 45nm is shown in Fig. 3(b), accompanied by obvious side lobes near the focal spot.

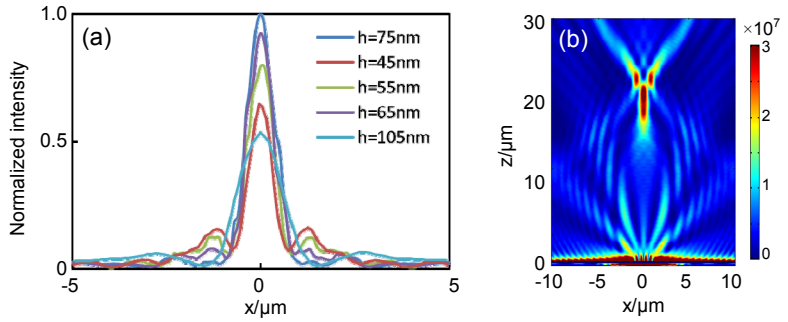

Fig. 3. (a) Intensity profile of the focal spot for the case with imperfect depth of the grooves. (b) Field maps of the structure with h = 45nm.

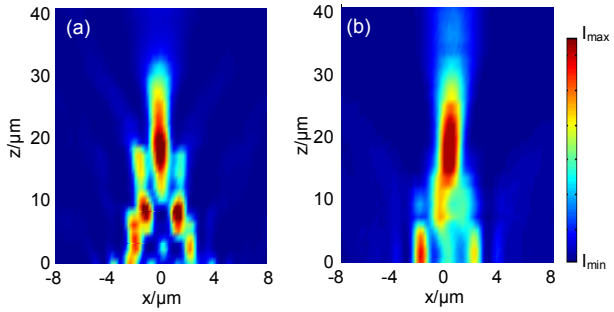

Fig. 4. Measured field maps for (a) d = 2.1μm and (b) d = 2.5μm.

Experimental results for d = 2.1μm and 2.5μm are also presented in Fig. 4. The field maps for d = 2.1μm and d = 2.89μm are very similar because of the periodicity of plasmon assisted two-slit transmission [19]. The longitudinal position of the focal point for d = 2.9μm is slightly further than that for d = 2.1μm while the position of the dark fringes of the main lobe depends on the distance between the two slits that affects the plasmon interference. In contrast, when d = 2.5μm, the nodes of the standing-wave pattern along the interface between the fiber core and gold film coincide with the slits and the SPP transmission is minimum. So, although the phase of two light beams at x = 0 is the same, the output intensity is very weak due to the lower efficiency of generating the Airy beam. In order to measure the interference field, the incident light power for d = 2.5μm is increased nearly fourfold compared to the other two cases.

#213846 - $15.00 USD Received 11 Jun 2014; revised 9 Jul 2014; accepted 10 Jul 2014; published 22 Jul 2014

2.2 Asymmetrical double Airy beams

All the discussions above correspond to the identical double Airy beams with opposite acceleration directions. In most cases, one may want to change the characteristics at the junction of the two main lobes, which can be realized by controlling the phase difference of the two light beams. Shifting grooves on the right side along the + x-direction can achieve different initial phase differences between two main lobes. The propagation dynamics of two Airy beams with opposite acceleration directions and different initial phase differences (0, π/4, π, 3π/2, 2π) are presented in Fig. 5(a). Figures 5(b) and 5(c) show the intensity profiles at the junction of the two main lobes and the dependence of the intersection distance of the main lobes on the phase difference. The junction of the main lobes of two beams is a dark core for the case of π phase difference. The brightest spot appears periodically at the junction of the main lobes. Within 0~2π phase difference, the brightest spot first appears on the right side of the junction of the main lobes, and then on the left side for increasing phase difference. The

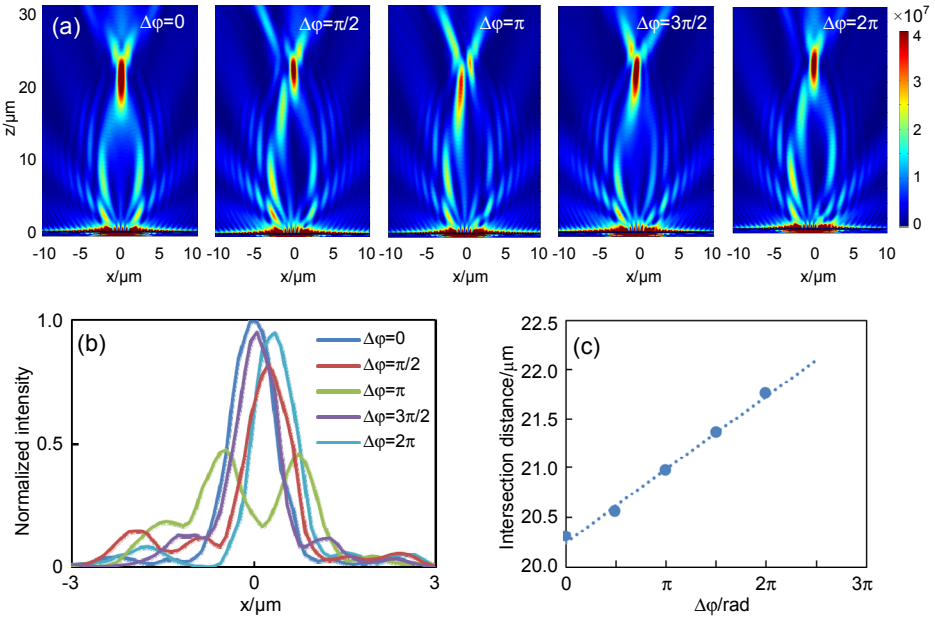

Fig. 5. (a) Field maps of symmetrical double Airy beams for different initial phase differences. (b) Intensity profiles at the junction of the two main lobes. (c) Dependence of the intersection distance of main lobes on the phase difference.

intersection distance of two main lobes is larger and shifts to + x direction with increasing phase difference, which contributes to the increase of the distance between two main lobes at z = 0. The generation efficiencies of the Airy beam on both sides are slightly different, which leads to a slightly asymmetrical field distribution.

3. Double orthogonal Airy beams

The propagation properties of two orthogonal Airy beams have also been investigated. Due to the limitation of the SMF core size, a multimode fiber (MMF) with a core diameter of 50μm is utilized. SEM images of a sample with two orthogonal Airy beams generator are shown in Figs. 6(a)-6(c). The two orthogonal air slits intersect at the center of the fiber core, where the length of slits and grooves is 7μm and the other parameters are the same as those in Fig. 1. In the experiment the input polarization direction was adjusted to be approximately 45° with respect to the direction of the two air slits, so that SPPs are equally excited in the two air slits. If the polarization direction is consistent with the direction of a slit, only a single Airy beam can be

#213846 - $15.00 USD Received 11 Jun 2014; revised 9 Jul 2014; accepted 10 Jul 2014; published 22 Jul 2014

generated. The cross sections of the captured beam images at different propagation distances along the z-axis are presented in Fig. 6(d). Two pure orthogonal Airy beams with three side lobes can be clearly observed at z = 1μm; no other interference fringes are present, unlike the case of two parallel Airy beams. The light intensity near the core center is slightly higher, due to the inhomogeneous distribution of the incident field. As the propagation distance z increases, the two Airy beams accelerate respectively along the orthogonal direction (the white arrows in Fig. 6(d)), similar to the 2D Airy beam [11], and then cross about at 25μm. Two Airy beams do not interfere because their polarization directions are perpendicular to each other and the interference fringes will not appear in the far field, which is totally different to the case of two parallel Airy beams.

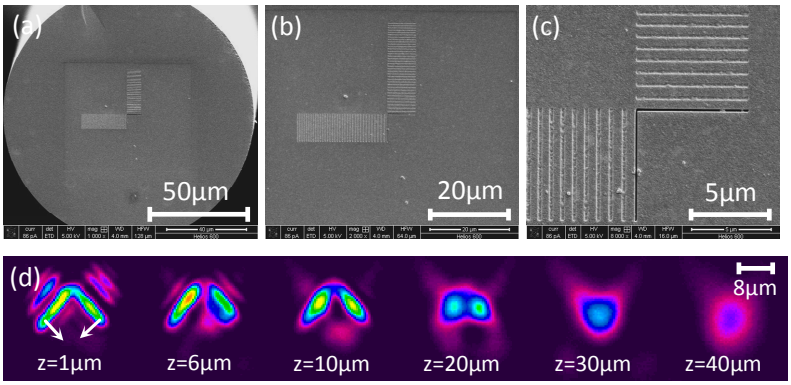

Fig. 6. (a)-(c) SEM images of the nanostructured gold coated optical fiber facet with two orthogonal slits and groove arrays. (d) Cross sections of the captured beam images at different propagation distances.

4. Conclusion

In summary, the propagation properties of compact all-fiber plasmonic multi-Airy beams have been investigated experimentally. The sub-wavelength self-focusing of double parallel Airy beams in free space has been observed experimentally and show good consistency with theoretical predictions. The nonuniform depth of the grooves greatly impacts on the intensity profile of the focal spot. The characteristics at the junction of the two main lobes can be adjusted by controlling the initial phase difference of the two Airy beams. The propagation of two orthogonal Airy beams has also been obtained. An all-fiber Airy beam generator provides many advantages, such as no need for alignment systems, high flexibility, lower insert loss, and easy portability. Multi-Airy beams are important to realize optical trapping, laser shaping, particle micromanipulation, and on-chip integration. Our results broaden the application of Airy beams and take it one step forward closer to practical applications.

Acknowledgment

This work was supported by the National Natural Science Foundation of China (NSFC) under Grant Nos. U1231201, 61275094, 11104043, 613111156, 61201083 and 11274077, partly by the Natural Science Foundation of Heilongjiang Province in China under Grant No. LC201424, by the Special Foundation for Harbin Young Scientists under Grant Nos. 2012RFLXG030 and 2013RFQXJ099, by Foundation for University Key Teacher by Heilongjiang province under Grant No. 1254G014, by the 111 project (B13015) to the Harbin Engineering University. G.B. gratefully acknowledges the Royal Society (London) for his University Research Fellowship and his International Exchanges Scheme with China. P.W. gratefully acknowledges Science Foundation Ireland (SFI) for the International Strategic Cooperation Award Grant No. SFI/13/ISCA/2845.

#213846 - $15.00 USD Received 11 Jun 2014; revised 9 Jul 2014; accepted 10 Jul 2014; published 22 Jul 2014